# $MmpL8_{MAB}$ controls *Mycobacterium abscessus* virulence and production of a previously unknown glycolipid family

Violaine Dubois[a], Albertus Viljoen[b,1], Laura Laencina[a,1], Vincent Le Moigne[a], Audrey Bernut[b,2], Faustine Dubar[c], Mickaël Blaise[b], Jean-Louis Gaillard[a,d], Yann Guérardel[c], Laurent Kremer[b,e], Jean-Louis Herrmann[a,d,3], and Fabienne Girard-Misguich[a,3]

[a]Université de Versailles Saint Quentin en Yvelines, INSERM UMR1173, 78000 Versailles, France; [b]CNRS UMR 9004, Institut de Recherche en Infectiologie de Montpellier, Université de Montpellier, 34293 Montpellier, France; [c]Université de Lille, CNRS UMR 8576, Unité de Glycobiologie Structurale et Fonctionnelle, 59000 Lille, France; [d]Assistance Publique-Hôpitaux de Paris, Groupement Hospitalier Universitaire Paris Ile de France Ouest, Hôpital Raymond Poincaré, Hôpital Ambroise Paré, 92380 Garches, Boulogne Billancourt, France; and [e]INSERM, Institut de Recherche en Infectiologie de Montpellier, 34293 Montpellier, France

Edited by D. Branch Moody, Brigham and Women's Hospital, Harvard Medical School, Boston, MA, and accepted by Editorial Board Member Carl F. Nathan September 7, 2018 (received for review July 31, 2018)

***Mycobacterium abscessus*** **is a peculiar rapid-growing** ***Mycobacterium*** **(RGM) capable of surviving within eukaryotic cells thanks to an arsenal of virulence genes also found in slow-growing mycobacteria (SGM), such as** ***Mycobacterium tuberculosis*****. A screen based on the intracellular survival in amoebae and macrophages (MΦ) of an** ***M. abscessus*** **transposon mutant library revealed the important role of MAB_0855, a yet uncharacterized Mycobacterial membrane protein Large (MmpL). Large-scale comparisons with SGM and RGM genomes uncovered MmpL12 proteins as putative orthologs of MAB_0855 and a locus-scale synteny between the** ***MAB_0855*** **and** ***Mycobacterium chelonae mmpL8*** **loci. A KO mutant of the** ***MAB_0855*** **gene, designated herein as** $mmpL8_{MAB}$**, had impaired adhesion to MΦ and displayed a decreased intracellular viability. Despite retaining the ability to block phagosomal acidification, like the WT strain, the** $mmpL8_{MAB}$ **mutant was delayed in damaging the phagosomal membrane and in making contact with the cytosol. Virulence attenuation of the mutant was confirmed in vivo by impaired zebrafish killing and a diminished propensity to induce granuloma formation. The previously shown role of MmpL in lipid transport prompted us to investigate the potential lipid substrates of** $MmpL8_{MAB}$**. Systematic lipid analysis revealed that** $MmpL8_{MAB}$ **was required for the proper expression of a glycolipid entity, a glycosyl diacylated nonadecyl diol (GDND) alcohol comprising different combinations of oleic and stearic acids. This study shows the importance of** $MmpL8_{MAB}$ **in modifying interactions between the bacteria and phagocytic cells and in the production of a previously unknown glycolipid family.**

MMPL | *Mycobacterium* | *abscessus* | glycolipid | GDND

One major feature of pathogenic mycobacteria is their ability to survive in phagocytic cells (1, 2), a property that is shared with the rapidly growing *Mycobacterium abscessus* (3, 4). The unique and lipid-rich mycobacterial cell envelope is largely responsible for the interactions with host immune cells, enabling the bacilli to resist the harsh conditions and bactericidal processes encountered within the macrophage (MΦ), such as phagosome maturation, nitrosative and oxidative stress, and nutrient deprivation (1, 2, 5–7). A large set of proteins participates in the biogenesis and transport of a wide diversity of cell wall-associated (glycol-)lipids (8–10). Impaired synthesis and/or transport of some of these lipids render pathogenic mycobacteria more susceptible to the host immune defenses (11–14). *Mycobacterium tuberculosis* mutants that fail to synthesize or transport the cell wall-associated phthiocerol dimycocerosates (PDIMs) show limited growth in the lungs of infected mice (11). The structurally related phenolic glycolipids (PGLs), which are unique to a few pathogenic species, are also required for optimal virulence in zebrafish of *Mycobacterium marinum*, a close pathogenic relative to *M. tuberculosis* (12, 15). Immune evasion by *M. tuberculosis* and *M. marinum* also seems to be mediated by PDIM, very likely through masking the underlying pathogen-associated molecular patterns, and by PGL through the involvement of a chemokine receptor 2-mediated pathway with preferential recruitment and infection of permissive MΦ while evading microbicidal ones (13).

In nontuberculous mycobacteria (NTM) such as *Mycobacterium avium*, a slow-growing *Mycobacterium* (SGM), or *M. abscessus*, a rapid-growing *Mycobacterium* (RGM), glycopeptidolipids (GPLs) play an important role in NTM physiology and behavior toward eukaryotic hosts (4, 16). A transition from a smooth (S) to a rough (R) morphotype in NTM is associated with GPL loss (17–19) that results in an exacerbated virulence phenotype in various cellular and animal models (20–23). Isolation of the R variant is often

## Significance

One major defense mechanism of mycobacteria relies mainly on the synthesis and transport of specialized lipids, processes that reside in the cell wall. Among the transporters, Mycobacterial membrane protein Large (MmpL) plays an essential role. We describe the role of MmpL8 ($MmpL8_{MAB}$) in the survival of *Mycobacterium abscessus* within eukaryotic hosts. We show that its absence slows the contact between *M. abscessus* and the host cell cytosol, an essential element in its resistance to the cell bactericidal mechanisms. The absence of $MmpL8_{MAB}$ leads to reduced production of a previously unknown glycolipid: a glycosyl diacylated nonadecyl diol (GDND). The glycolipid seems unique to the *Mycobacterium chelonae* complex, supporting the view that GDND might represent a typical signature of *M. abscessus* infection.

Author contributions: J.-L.G., Y.G., L.K., J.-L.H., and F.G.-M. designed research; V.D., A.V., L.L., V.L.M., A.B., F.D., and Y.G. performed research; M.B. contributed new reagents/analytic tools; V.D., A.V., A.B., F.D., Y.G., L.K., J.-L.H., and F.G.-M. analyzed data; and V.D., A.V., Y.G., L.K., J.-L.H., and F.G.-M. wrote the paper.

The authors declare no conflict of interest.

This article is a PNAS Direct Submission. D.B.M. is a guest editor invited by the Editorial Board.



[1]A.V. and L.L. contributed equally to this work.

[2]Present address: Bateson Centre, Department of Infection, Immunity and Cardiovascular Disease, University of Sheffield, S10 2RX Sheffield, United Kingdom.

[3]To whom correspondence may be addressed. Email: jean-louis.herrmann@aphp.fr or fabienne.misguich@uvsq.fr.

This article contains supporting information online at www.pnas.org/lookup/suppl/doi:10.1073/pnas.1812984115/-/DCSupplemental.

Published online October 9, 2018.

associated with chronic and more severe disease in patients with reduced pulmonary functions (4, 24–26). This is exemplified in the case of *M. abscessus*, where the transition to an R morphotype is sufficient to confer a highly virulent phenotype in zebrafish or mice (27, 28).

However, we recently showed, by looking at the differential intracellular behavior of both S and R *M. abscessus* variants, that GPLs confer a clear intracellular survival advantage to the S variant compared with the R variant, including resistance to several cellular antibacterial mechanisms, such as blockage of phagosomal acidification, and resistance to apoptosis and autophagy (4, 7). Complementary to our study, GPLs were shown to inhibit apoptosis in *M. abscessus*-infected MΦ by interacting with the mitochondrial cyclophilin D (29).

These results further highlight how mycobacterial lipids fine tune MΦ–*M. abscessus* interactions to modulate the host immune response. However, GPLs are common to all NTM, SGM, and RGM, and *M. abscessus* belongs to the RGM group that comprises mainly saprophytic species. However, unique lipids possibly involved in the peculiar pathogenicity of *M. abscessus* remain to be identified.

To act as critical players in mycobacterial pathogenesis, these complex lipids, usually synthesized within the cytoplasm, need to be translocated through the cell envelope and exposed to the bacterial surface, a process that can require a wide repertoire of lipid-specific transporters. Gap, a transmembrane protein participating in the transport of GPL through the plasma membrane, was originally identified in *Mycobacterium smegmatis* (18). The last decade has seen a mounting focus on the Mycobacterial membrane protein Large (MmpL) permeases, which are a subclass of the Resistance-Nodulation-cell-Division proteins containing 12 transmembrane domains (TMDs) and are known to translocate lipids through the plasma membrane (30–32). Complex lipids thought to be transported by MmpL proteins include PDIM (MmpL7), sulfoglycolipid (MmpL8), diacyltrehaloses (DATs) and polyacyltrehaloses (MmpL10), monomeromycolyl diacylglycerol (MmpL11), and trehalose monomycolate (MmpL3), all of which have been implicated in *M. tuberculosis* virulence (31, 32). Additionally, the essential MmpL3 transporter represents a promising pharmacological target in *M. tuberculosis* and *M. abscessus* (33–35). In *M. abscessus*, we and others unraveled the specific role of MmpL4a and MmpL4b in GPL transport by analyzing the S to R transition in the three subspecies of the *M. abscessus* complex (17, 22, 36). These MmpLs represent the only MmpL actors described so far in *M. abscessus* virulence, despite the greater abundance of MmpLs in the *M. abscessus* complex (4). Another group of lipids, the trehalose-based polyphleates, present in many NTM (37) has recently been proposed to contribute to the highly aggregative phenotype of *M. abscessus* R (38), but a direct role in *M. abscessus* virulence remains to be shown.

In continuation of our previous efforts to decipher the mechanisms of pathogenicity of *M. abscessus*, we recently performed a phenotypic screen of a transposon (*Tn*) mutant library generated in *M. abscessus* subspecies (subsp.) *massiliense* in amoebae and MΦ. This led to the discovery of the role of the ESX-4 type VII secretion system (T7SS) in intracellular survival of *M. abscessus* (39). This genetic screen also disclosed the *MAB_0855* gene, encoding a yet uncharacterized MmpL. Herein; we aimed at characterizing this MmpL, designated MmpL8$_{MAB}$, as well as its putative lipid substrate. We show the crucial role of MmpL8$_{MAB}$ in intracellular survival and virulence of *M. abscessus* in various cellular and animal models. We also present a structural description of a glycolipid family produced at reduced levels in the absence of MmpL8$_{MAB}$, thereby opening the way to promising future translational applications.

## Results

**Identification of an *mmpL* Gene Crucial for Intracellular Survival of *M. abscessus*.** A *Tn* mutant library constructed in the *M. abscessus* subsp. *massiliense* 43S clinical isolate was originally screened for survival in *Acanthamoeba castellanii* amoebae and in J774.2 murine MΦ (39); 7 of 47 mutants that exhibited a Growth Index (GI) below 0.5 in MΦ compared with the WT strain carried a single *Tn* insertion in genes involved in cell wall/membrane/envelope assembly and/or lipid transport and metabolism as determinated by cluster of orthologous groups (COG) analysis (COG M and I, respectively) (Fig. 1 and Table 1). Interestingly, one mutant (55F6) was highly attenuated in both amoeba and MΦ (GIs of 0.13 and 0.31, respectively) and was linked to only a general function (COG R) (Fig. 1). By sequencing the *Tn* insertion site, we identified the *Tn*-disrupted gene as *MYCMA_0439* (*SI Appendix*, Table S1), identical to the *M. abscessus* subsp. *abscessus* ATCC19977 *MAB_0855* gene, which according to systematic annotation, encodes a putative MmpL protein. The 55F6 mutant's intracellular defect was further confirmed by survival kinetics performed in amoebae and MΦ by determining the cfu and the corresponding GIs (0.18 in amoebae and 0.22 in MΦ) (*SI Appendix*, Fig. S1).

**MAB_0855 Is Unique to the *Mycobacterium chelonae* Complex.** Primary sequence analysis and 3D homology modeling indicate that MAB_0855 presents the typical features of MmpL transporters, possessing 12 helical TMDs as well as two extracytoplasmic loops between TMD1/2 and TMD7/8, which are potentially implicated in substrate binding (*SI Appendix*, Fig. S2).

Phylogenetic relationships among 31 MmpLs of *M. abscessus* and 13 MmpLs of *M. tuberculosis* allowed the identification of two *M. abscessus* MmpL-specific clades (light blue and red spots in Fig. 2*A*), supporting the hypothesis of MmpL diversification in *M. abscessus* (31). Tandem duplications occurred as illustrated by the *mmpL4* genes (*mmpL4a* and *mmpL4b*) (blue brackets in Fig. 2*A*). MAB_0855 clustered with *M. tuberculosis* MmpL8 and MmpL12 and to a lesser extent, with *M. tuberculosis* MmpL10 and *M. abscessus* MAB_0937c (dark blue spot in Fig. 2*A*). MAB_0937c is orthologous to MmpL10 in both RGM and SGM (Fig. 2*B*). Neither phylogenetic reconstruction nor Bidirectional Best Hit (BBH) search found putative orthologs of MAB_0855 in *M. tuberculosis* (Fig. 2 *A* and *B*). However, an extensive mycobacterial BBH search identified MmpL12 proteins in *Mycobacterium kansasii*, *Mycobacterium gastri*, *M. smegmatis*, and *Mycobacterium mucogenicum* as putative orthologs to MAB_0855 (Fig. 2*B*). It is worth noting that, in these mycobacterial species, MmpL12 was suggested to transport lipooligosaccharides (LOSs) (40), which are absent in *M. abscessus*. MAB_0855 Best Hit (BH) scores were low (under 60) except in the *M. chelonae* complex (MCC; i.e., comprising the *M. abscessus* subspecies and *M. chelonae*) and in *Mycobacterium immunogenum*, for which the BH score was up to 96 (Fig. 2*B*). Finally, we failed to identify any syntenic conservation in other mycobacteria of the region spanning from *MAB_0852* to *MAB_0859*, with the exception of the *M. chelonae mmpL8* locus (Fig. 2*C*); therefore, MAB_0855 was designated *mmpL8$_{MAB}$*. Quite notably, several genes from *M. tuberculosis* were syntenic to the *M. abscessus* genome upstream of *MAB_0852* and downstream of *MAB_0859*, suggesting that a deletion may have occurred between these genes in *M. tuberculosis*, perhaps as a consequence of the genomic reduction that occurred in the tubercle bacillus (Fig. 2*C*).

Overall, the *mmpL8$_{MAB}$* genomic environment revealed a potential role in lipid biogenesis/transport, with a putative lipase/esterase encoding gene (*lipP*) as well as two *fad* genes (*fadA* and *fadB*) located upstream of *mmpL8$_{MAB}$* (Fig. 2*C*). A polyketide synthase (*pks*)-associated gene (*papA2*) as well as a putative polyketide cyclase gene (*MAB_0859*), possibly participating in the biogenesis and assembly of a complex cell wall lipid (41), were also found in close proximity to *mmpL8$_{MAB}$*.

**MmpL8$_{MAB}$ Plays a Critical Role in *M. abscessus* Intracellular Survival and Virulence.** To confirm the contribution of MmpL8$_{MAB}$ to *M. abscessus* virulence, deletion mutants were generated in both the

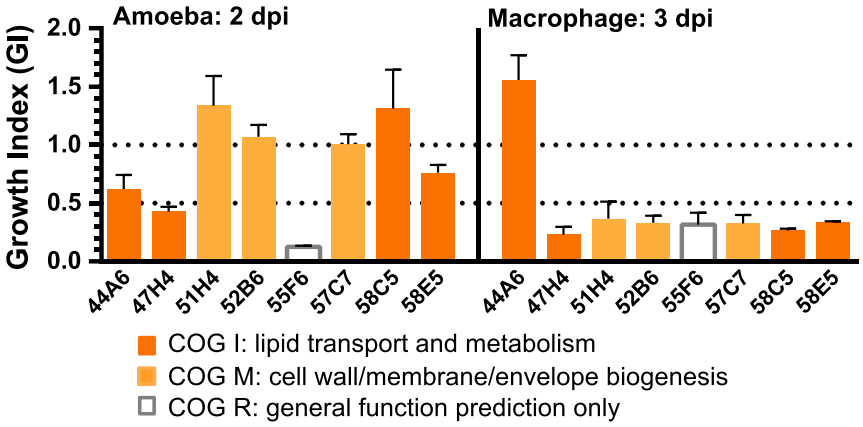


**Fig. 1.** Identification of a putative MmpL required for intracellular replication in both amoebae and MΦ from a *Tn* library screen. *Tn* mutants impaired in their intracellular survival compared with the WT strain GI in amoebae and MΦ. Amoebae (*A. castellanii*) and murine MΦ were infected at an MOI of 10 and lysed at different dpi (2 and 3 dpi, respectively) before cfu determination. The *Tn* insertion site was cloned to identify the disrupted genes. Identified genes were categorized with the COG classification. Mutants for which the *Tn* insertion occurred in a gene implicated in either lipid metabolism/transport or related processes (COG M and I, respectively) and 55F6 uncharacterized (COG R) mutant putatively implicated in lipid transport and metabolism are depicted.

S and R variants of the *M. abscessus* ATCC19977-type strain by allelic exchange of the $mmpL8_{MAB}$ ORF using the recombineering strategy (42, 43) that replaces genes targeted for deletion with a zeocin resistance cassette (*SI Appendix*, Fig. S3). The proper deletion of $mmpL8_{MAB}$ was subsequently confirmed through a combination of PCR and sequencing analyses (*SI Appendix*, Fig. S3). The corresponding mutant strains generated in the S or R background, hereafter referred to as S$\Delta mmpL8_{MAB}$ or R$\Delta mmpL8_{MAB}$, were complemented by transformation with an integrative plasmid containing an intact copy of $mmpL8_{MAB}$.

S$\Delta mmpL8_{MAB}$ exhibited a pronounced defect in intracellular survival in murine MΦ compared with the WT or S$\Delta mmpL8_{MAB}$-complemented strains, and this alteration was already significant at 1 day postinfection (dpi) (Fig. 3*A*). Functional complementation of the mutant with the $mmpL8_{MAB}$ gene ($\Delta mmpL8$::$mmpL8_{MAB}$) fully restored the WT phenotype, whereas complementation with the *Mycobacterium massiliense* homolog *MYCMA_0439* ($\Delta mmpL8$::$0439_{MMAS}$) only partially restored the effect (Fig. 3*A*). These results indicate that the decreased viability of $\Delta mmpL8_{MAB}$ was not caused by a polar effect on the expression of the downstream genes. To get more insight into the biological functions of *mmpL8*, we addressed whether the three "closest" homologs found in *M. tuberculosis* (i.e., *mmpL8*, *mmpL10*, and *mmpL12*) (Fig. 2*A*) may restore the intracellular defect of $\Delta mmpL8_{MAB}$. As shown in Fig. 3*B*, a near-complete restoration of intracellular growth was obtained with the $mmpL8_{MTB}$ and $mmpL12_{MTB}$ genes but not with $mmpL10_{MTB}$. The intracellular growth defect of R$\Delta mmpL8_{MAB}$ was also fully restored on complementation with $mmpL8_{MAB}$ (Fig. 3*C*).

Overall, these results show that $MmpL8_{MAB}$ is required for the intracellular survival of both *M. abscessus* variants.

**$\Delta mmpL8_{MAB}$ Presents a Reduced Adhesion to MΦ and Is Impaired in Phagosome-Membrane Rupture.** The intracellular behavior of *M. abscessus* resembles the intracellular lifestyle of a slow-growing pathogenic species (4). In particular, scrutinizing the S and R forms in MΦ highlighted the importance of the outer cell wall layer in defining important physiological and ultrastructural features of the phagosomal compartment/membrane. Disruption of the phagosomal membrane enables the escape of the S variant to establish cytosolic communications, thereby contributing to survival inside the host cells (4). In line with these earlier findings, we investigated the possible mechanism(s) by which MmpL8 may interact with MΦ.

The question of whether MmpL8 affects the adhesion of the bacilli to the MΦ surface was determined by measuring the adhesion capacity of S$\Delta mmpL8_{MAB}$ to MΦ using flow cytometry. Cells with adherent bacteria formed a population that was well separated from the nonadherent bacteria together with cellular debris (Fig. 4*A*). A reproducible and significant twofold decrease in $\Delta mmpL8_{MAB}$ cell adhesion was observed compared with WT and complemented strains (Fig. 4*A*).

We next addressed whether a functional $MmpL8_{MAB}$ participates in the inhibition of phagosomal acidification, known as a crucial event for intra-MΦ survival of pathogenic mycobacteria (44). As shown in Fig. 4*B*, WT *M. abscessus*, but not the heat-killed strain, inhibited the intraphagosomal pH as reported previously (4). $\Delta mmpL8_{MAB}$ blocked phagosomal acidification in a manner similar to the WT and $\Delta mmpL8_{MAB}$-complemented strains (Fig. 4*B*). This indicates that it is very unlikely that the reduced intracellular survival of $\Delta mmpL8_{MAB}$ is connected to a defect in phagosomal acidification and the subsequent maturation of the phagolysosome compartments.

To address the potential role of $MmpL8_{MAB}$ in phagosomal membrane damage that leads to cytosolic communications, we carried out an FRET-based assay recently adapted for *M. abscessus* that allowed us to assay phagosomal membrane disruption (4). At 20 h postinfection (hpi), $\Delta mmpL8_{MAB}$ was significantly reduced in its ability to damage the phagosomal membrane, and this persisted for longer time points (30 hpi) compared with the WT and $\Delta mmpL8_{MAB}$-complemented strains (Fig. 4*C*). To further confirm the inability of $\Delta mmpL8_{MAB}$ to establish contacts with the cytosol, we evaluated the production of IL-1β (Fig. 4*D*), documented as a biomarker of cytosolic *M. tuberculosis* (45–49). Consistently

**Table 1. Genes disrupted by *Tn* insertion in *M. massiliense* 43S; attenuated in MΦ; and with a potential implication in cell wall assembly, lipid transport, and metabolism**

| *Tn* mutants | *Tn*-disrupted gene and corresponding encoded protein | Corresponding gene and encoded protein in *M. abscessus* |
|---|---|---|
| 44A6 | *MYCMA_2469: fabG* | *MAB_4443*: probable 3-oxoacyl-[acyl-carrier protein] reductase |
| 47H4 | *MYCMA_09125*: modD | *MAB_2436*: conserved hypothetical protein |
| 51H4 | *MYCMA_08185*: mammalian cell entry protein *mce* | None |
| 52B6 | *MYCMA_0991*: nitrate ABC transporter substrate-binding protein | *MAB_1915*: probable fatty acid-CoA ligase FadD |
| 55F6 | *MYCMA_0439*: membrane protein | *MAB_0855*: putative membrane protein, MmpL family |
| 57C7 | *MYCMA_2554*: acyl-CoA synthetase | *MAB_4626c*: probable fatty acid-CoA ligase FadD |
| 58C5, 58E5 | *MYCMA_0056*: oxydoreductase | *MAB_0090c*: probable oxidoreductase EphD |

MICROBIOLOGY

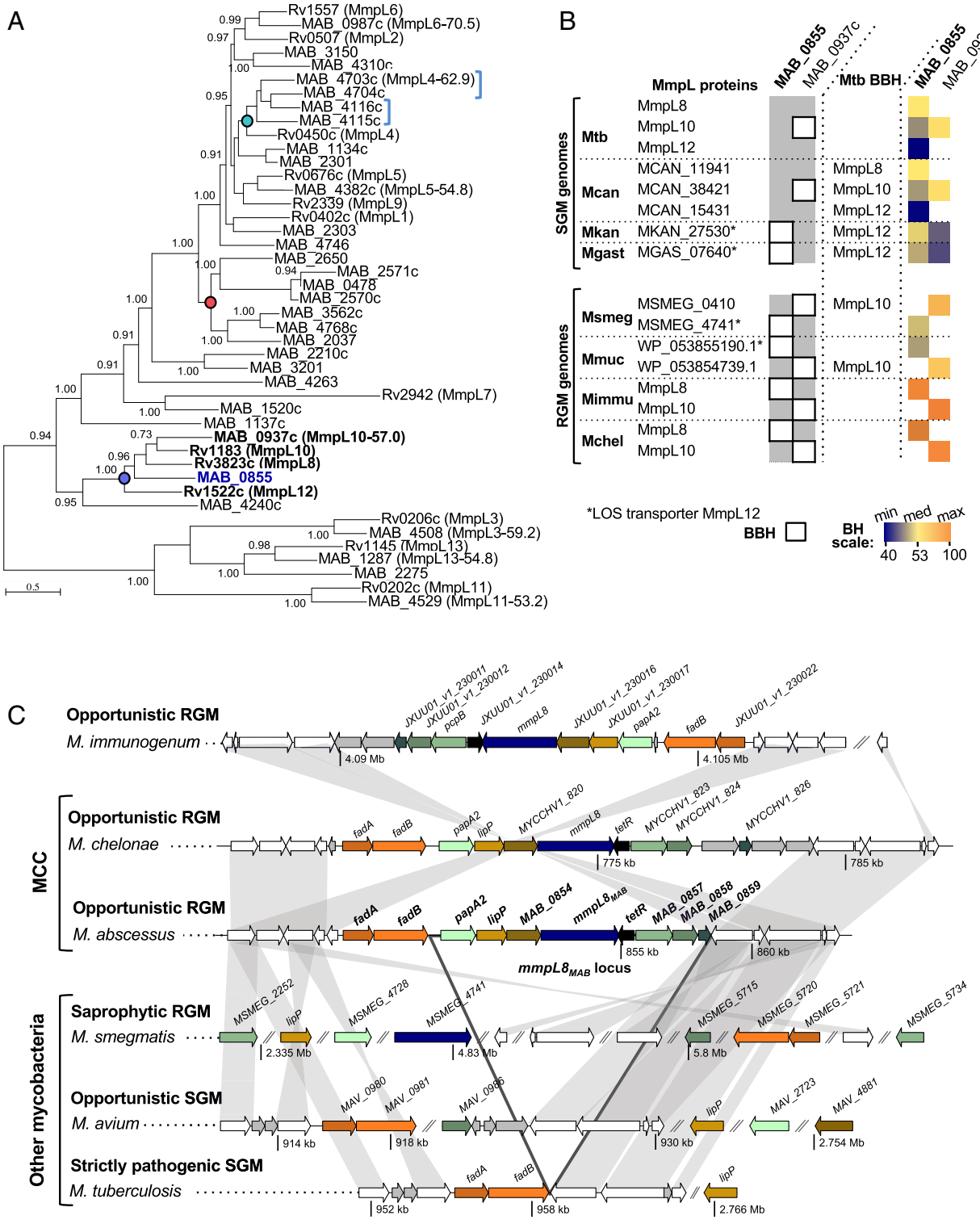


**Fig. 2.** MAB_0855 transporter is specific to the MCC. (*A*) MAB_0855 phylogenetic position among *M. tuberculosis* MmpL transporters. In this study, BH scores were calculated with the Opscan program. A BBH between two proteins corresponds to a putative ortholog. *M. abscessus* and *M. tuberculosis* MmpL phylogeny was inferred by Maximum Likelihood using the PHYML software and the aLRT statistic from the Multiple Sequence Alignment of *M. abscessus* and *M. tuberculosis* performed with Clustal. The aLRT statistical values over 0.9 are indicated. When a BBH was found between two proteins, the BBH score is indicated in brackets. (Scale bar: 0.5 estimated amino acid substitutions.) (*B*) Conservation of MAB_0855 in mycobacteria. MAB_0855 and MAB_0937c BBHs with MmpL proteins outside *M. abscessus* strains are represented by check boxes (*Left*). BBHs of these foreign MmpLs with *M. tuberculosis* MmpLs, if any, are indicated (*Center*). MAB_0855 and MAB_0937c hit scores, which give a clue on MAB_0855 and MAB_0937c level of conservation among mycobacteria, are also depicted by a range of colors (*Right*). The lowest scores are depicted in blue; the highest scores are depicted in orange. (*C*) Conservation of *MAB_0855* locus among pathogenic and nonpathogenic mycobacteria. The chromosomal loci encompassing the relevant genes depicted in the figure were built with the GenoPlotR package. Genes for which no BBHs were found are depicted in gray. Genes exhibiting BBH toward *MAB_0855* locus genes and the two *fad* genes upstream of the locus are depicted in color. A gray band links other BBH genes (in white).

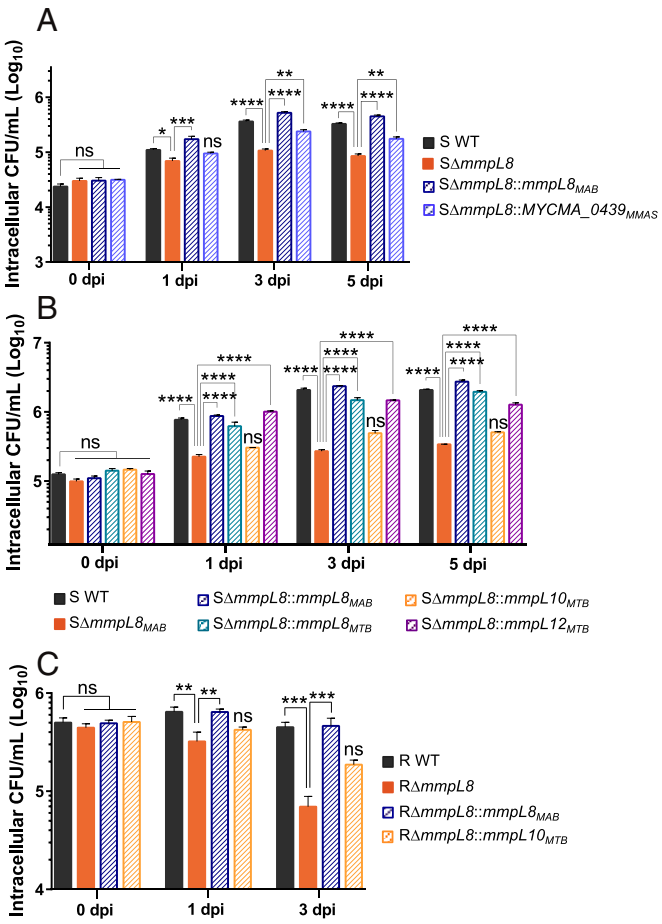


**Fig. 3.** Elucidation of the *mmpL8*$_{MAB}$ role in *M. abscessus* virulence. Intracellular growth was assessed by cfu counting throughout the infection. Murine MΦ were infected at 10 MOI with the SΔ*mmpL8*$_{MAB}$ or with the complemented strain carrying the *MYCMA_0439* or the *mmpL8*$_{MAB}$ gene (*A*), the *M. tuberculosis*-closest homologs to *M. abscessus mmpL8* (*mmpL8*$_{MTB}$, *mmpL10*$_{MTB}$, *mmpL12*$_{MTB}$; *B*), or *mmpL10*$_{MTB}$ (*C*); cfu histograms with error bars represent means ± SD calculated using data from three independent experiments. Differences between means were analyzed by two-way ANOVA and the Tukey posttest, allowing multiple comparisons. ns, Non-significant. *$P < 0.05$; **$P < 0.01$; ***$P < 0.001$; ****$P < 0.0001$.

with the FRET data, Δ*mmpL8*$_{MAB}$ was less potent at inducing IL-1β production by infected MΦ compared with WT and Δ*mmpL8*$_{MAB}$-complemented strains. This effect, already seen at 3 hpi, persisted for at least 30 hpi and was dependent on the caspase-1 pathway, as shown in *SI Appendix*, Fig. S4*A*, and based on the presence of the mature form of IL-1β (*SI Appendix*, Fig. S4*B*), it was not an artifact.

Taken collectively, these results indicate that the inactivation of MmpL8$_{MAB}$ reduces its interaction with MΦ as well as its ability to enter the cells; it also impairs the establishment of cytosolic connections. Whether these cellular phenotypes are translated into attenuation was next investigated using the recently developed zebrafish model of infection (28).

**MmpL8$_{MAB}$ Is Essential for Full Virulence of *M. abscessus* in Zebrafish.** Since *M. abscessus* R induces a more robust and lethal infection in zebrafish compared with the S form (28, 50, 51), embryos were infected with WT, RΔ*mmpL8*$_{MAB}$, and complemented strains before the determination of the survival curves. While the R WT strain led to rapid larval death (~80% killing at 13 dpi) as reported previously (28), Δ*mmpL8*$_{MAB}$, which has retained its propensity to produce cords (*SI Appendix*, Fig. S5), was attenuated in its virulence (~30% killing at 13 dpi) (Fig. 5*A*). Reintroduction of a functional copy of the gene into Δ*mmpL8*$_{MAB}$ partially restored the virulent phenotype to the level of the WT strain, thus linking MmpL8$_{MAB}$ to *M. abscessus* virulence in zebrafish.

In addition to cording, a phenotypical trait conferring virulence to the R variant in zebrafish (51) is granuloma formation, which also represents a physiopathological sign of *M. abscessus* infection in embryos, although it has been reported to occur in both S and R variants (22, 28). We thus compared granuloma formation after infection with WT R and S variants and Δ*mmpL8*$_{MAB}$ R and S mutants. A striking reduction in the number of embryos with granulomas (Fig. 5*B*, *Left*) as well as in the number of granulomas per embryo (Fig. 5*B*, *Right*) was observed in Δ*mmpL8*$_{MAB}$-infected embryos. Partial restoration of the WT phenotype (embryos with granulomas and number of granulomas per embryo) was observed with the Δ*mmpL8*$_{MAB}$-complemented strain (Fig. 5*B*). These diminished pathological signs were unrelated to the morphotype of the mutant. Granuloma production is usually associated with chronic rather than with acute infection. Therefore, this phenotypic characteristic is probably not incriminated in the increased survival of the embryos infected with the mutant. However, since granuloma formation is a consequence of cellular aggregation often linked to the surface properties of the mycobacterial cell wall and/or the release of granulomatogenic compounds, notably lipids (52), these results raise the question whether specific modifications on the outer layer of *M. abscessus* are connected to a specific lipid exported by MmpL8$_{MAB}$.

**MmpL8$_{MAB}$ Is Required for Production of a Glycolipid.** A systematic TLC-based approach for the whole range of apolar and polar lipids was implemented; 1D TLC enabled the separation of abundant glycolipids, such as GPL and trehalose dimycolate, and allowed the identification of a chaplet of lipids with amounts that seemed to be severely decreased in mutant 55F6 compared with its *M. massiliense* 43S parental strain (brackets) (Fig. 6*A*, lanes 1 and 2). The same chaplet of lipids, with expression level that was affected in 55F6, was also decreased in SΔ*mmpL8*$_{MAB}$ mutants compared with their WT progenitors (Fig. 6*A*, lanes 3 and 4), and partial restoration of the phenotype was observed for the complemented S strain (Fig. 6*A*, lane 5). In particular, the abundance of one lipid assumed to be exported by MmpL8$_{MAB}$, migrating close to the GPL, was markedly different between mutant and WT strains, which was especially apparent in the R background devoid of GPL (Fig. 6*B*, lanes 3 and 4). Restoration of the phenotype was also observed for the complemented strain (Fig. 6*B*, lane 5). Restoration of lipid production was further confirmed when *M. tuberculosis mmpL8* and *-12*, but not *M. marinum mmpL7*, were used to complement Δ*mmpL8*$_{MAB}$ (*SI Appendix*, Fig. S6).

**The MmpL8$_{MAB}$ Putative Substrate Is a Glucose-Containing Lipid.** To get insights into the structure of the MmpL8$_{MAB}$ substrate, the lipid was first purified from the polar lipid fraction of *M. abscessus* as a homogenous lipid fraction, Pa3 (Fig. 6*C* and *SI Appendix*, Fig. S7). Monosaccharide and lipid composition analyses of the product showed the presence of glucose (*SI Appendix*, Fig. S8), hexadecanoic (C16), and octanoic acid (C18), which established the presence of a glucose-based glycolipid substituted by C18 and C16. MALDI-MS analysis of the Pa3 lipid fraction showed a complex pattern of signals with 28-amu increments dominated by signals at *m/z* 959, 987, and 1015 (Fig. 6*D*) tentatively attributed to $[M + H]^+$ ions of $Glc_1(C16)_2$, $Glc_1(C16)_1(C18)_1$, and $Hex_1(C18)_2$, respectively, all substituted by a yet unknown lipid moiety. $MS^2$ fragmentation of parent ions at *m/z* 987 showed that one Glc residue, one C18, and one C16 could be independently cleaved from the parent ion. C16 and C18 could be further independently cleaved from the $[M\text{-}Hex + H]^+$ fragment ion as established by $MS^3$ fragmentation of the fragment ion at *m/z* 825. This shows that C16 and C18 do not

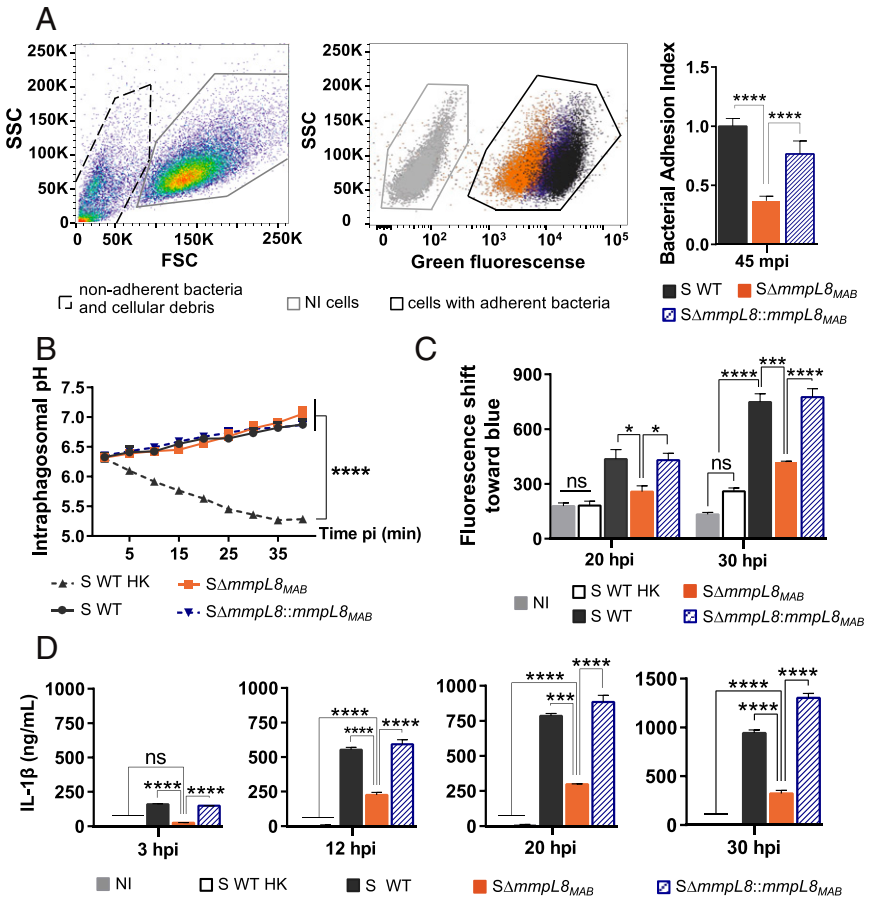


**Fig. 4.** $MmpL8_{MAB}$ plays a crucial role in *M. abscessus* interactions with cells by modulating *M. abscessus* entry and its survival inside the cells. (*A*) Adhesion to murine MΦ assessment by flow cytometry. MΦ were cooled down to avoid bacterial internalization and then infected with CFDA-SE–stained bacteria at an MOI of 100 for 1 h at 4 °C with gentle agitation to favor bacteria-to-cell contact. Nonadherent bacteria were well separated from intact cells (*Left*), and a substantial shift was observed for the cell population with adherent bacteria (*Right*; infected cells). The bacterial adhesion index is given that represents the mean fluorescence intensity (MFI) of each population with adherent bacteria reported to the MFI of the cells infected with the WT strain. FSC represents forward scatter and SSC represents side scatter. NI represents noninfected cells. (*B*) Phagosome acidification test. MΦ intraphagosomal pH after infection at an MOI of 10 was assessed by the mean FITC fluorescence measurement (485 nm) combined with mCherry fluorescence (565 nm) of double-stained bacteria. The pH along the infection is extrapolated from a pH standard curve. HK corresponds to heat killed bacteria. (*C*) Intracellular behavior in human THP-1. Cells were infected at an MOI of 10. The ability of bacteria to establish a contact with the cell cytosol was assessed by FRET at 20 and 30 hpi. (*D*) Kinetics of IL-1β production during THP-1 MΦ infection. The cellular response to infection with *M. abscessus* WT, $\Delta mmpL8_{MAB}$, and complemented strains was assessed by quantifying IL-1β secretion. Histograms with error bars represent means ± SD calculated using data from three independent experiments. Differences between means were analyzed by ANOVA and the Tukey posttest, allowing multiple comparisons to be performed. ns, Nonsignificant. $^{*}P < 0.05$; $^{***}P < 0.001$; $^{****}P < 0.0001$.

esterify the Glc residue. Finally, $MS^4$ fragmentation of the $MS^3$ fragment ion $[M\text{-}Hex\text{-}C18 + H]^+$ at *m/z* 541 generated a fragment ion at *m/z* 285 (Fig. 6*D*) that could be equally assigned to $[M + H]^+$ ions of octanoic acid $CH_3(CH_2)_{16}COOH$ or of nonadecyl alcohol $CH_3(CH_2)_{18}OH$. NMR analysis of the carbohydrate moiety showed the presence of a heterogeneous H1/C1 signal at $\delta^1H/^{13}C$ 50.6–5.2/94.2 that correlates on $^1H$-$^1H$ total correlated spectroscopy (TOCSY) and $^1H/^{13}C$ heteronuclear single quantum coherence (HSQC)-TOCSY spectra with an H2/C2 to H6/C6 monosaccharide spin system assigned as α-Glc*p* in a terminal nonreducing position (Fig. 6*E*), which establishes that the major Glc residue is not esterified on any carbon. Accordingly, the absence of a β-anomeric signal further suggests that the C1 position of α-Glc*p* is involved in an *O* linkage. However, the low available quantity of compound precluded the $^1H$-$^1H$ nuclear overhauser effect (NOe) transfer from the anomeric proton or $^3J_{H,C}$ connections by an $^1H$-$^{13}C$ heteronuclear multiple-bond correlation (HMBC) experiment, and thus, a final proof of the αGlc*p*-O-$CH_2$-R linkage could not be provided.

As aforementioned, structural analysis by NMR data and $MS^n$ fragmentation patterns suggest that the lipid is composed of an alkyl α-glucopyranoside substituted by a C19 alkane chain diesterified by two fatty acid chains. The fragmentation pattern of the parent ion at *m/z* 987 established that it is substituted by one palmitic and one stearic acid (Fig. 6*D*), whereas the parent ion at *m/z* 959 is substituted by two palmitic acid chains (*SI Appendix*, Fig. S9). The exact position of esterification sites on the alkyl chain could not be directly established by NMR due to low quantities. Finally, the observation of three $^1H/^{13}C$ signals with deshielded protons at δ 5.38/72.3, 5.18/69.4, and 5.061/68.51 (Fig. 6*E*) strongly suggests the presence of other forms of the lipid in which the Glc ring carbons are differentially acetylated. This would retrospectively explain the chemical shift heterogeneity of the anomeric signal of the αGlc*p* residue.

In summary, structural analyses established that the major lipid with production that is severely affected by $MmpL8_{MAB}$ deficiency consists of a heterogeneous family of Glc-containing lipids in which Glc is linked to a diacylated lipid. All of the data are consistent with the presence of a Glc alkylated with a C19 diol esterified by different combinations of palmitic and stearic acids (Fig. 6*D*), but they do not exclude the presence of additional related compounds with further acylation sites on the glucose residue.

## Discussion

NTM have recently emerged as important opportunistic pathogens responsible for severe lung diseases. Several studies have reported the predominance of *M. abscessus* among RGM in patients with cystic fibrosis (CF), chronic obstructive pulmonary disease (53), underinhaled corticosteroid therapy, and bronchiectasis (21, 54–58). The deleterious impact of *M. abscessus* in the degradation of lung function in CF patients has also been well documented (26). To dissect important and specific mechanisms of pathogenesis and to identify virulence determinants, we recently screened a *Tn* mutant library in *A. castellanii* and uncovered genes essential for *M. abscessus* intracellular survival (39). This approach unraveled the crucial and unexpected role of the ESX-4 locus for intracellular survival and phagosomal escape (39). In continuation of these efforts, we present here the discovery and preliminary characterization of *MYCMA_0439* as an additional factor required for the intracellular survival of *M. abscessus* in both amoebae and MΦ. By focusing on its *M. abscessus* subsp. *abscessus* counterpart (*MAB_0855*, $mmpL8_{MAB}$), we confirmed the contribution of $MmpL8_{MAB}$ in *M. abscessus* virulence by first generating an $mmpL8_{MAB}$ deletion mutant ($\Delta mmpL8_{MAB}$) and subsequently showing for this mutant attenuation in intracellular survival, delayed cytosolic escape, and a

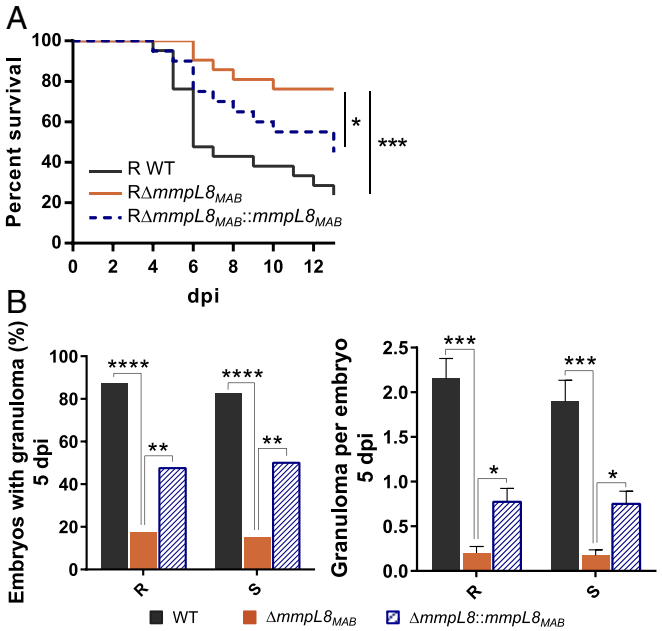


**Fig. 5.** The *mmpL8* gene plays a role in *M. abscessus* in vivo survival and virulence. (*A*) Survival curves of embryos. Embryos were injected into the bloodstream with 200 cfu of tdTomato-expressing *M. abscessus* R (parental strain), R$\Delta mmpL8_{MAB}$ mutant, or the complemented strain R$\Delta mmpL8$::$mmpL8_{MAB}$ ($n$ = 20). Data are representative of two independent experiments. (*B*) Kinetics of granuloma formation. Embryos were i.v. infected with 200 cfu of tdTomato-expressing *M. abscessus* R, *M. abscessus* S, R$\Delta mmpL8_{MAB}$, S$\Delta mmpL8_{MAB}$ mutants, S$\Delta mmpL8$::$mmpL8_{MAB}$, or R$\Delta mmpL8$::$mmpL8_{MAB}$. Granulomas were then counted at 5 dpi. Histograms represent means ± SEM values calculated from two independent experiments. The statistical test used was the Fisher's exact test (*Left*), and means were analyzed by ANOVA and the Tukey posttest (*Right*). *$P < 0.05$; **$P < 0.01$; ***$P < 0.001$; ****$P < 0.0001$.

reduced capacity to provoke zebrafish killing. Direct implication of *MAB_0855* (*mmpL8*$_{MAB}$) in these impaired virulence phenotypes was confirmed by functionally complementing the mutant phenotypes.

MmpL contribution to mycobacterial virulence was first reported in *M. tuberculosis* by the screening of a *Tn* mutant library for in vivo survival deficiency (59). Genetic disruptions in *M. tuberculosis mmpL4*, *-5*, *-7*, *-8*, *-10*, and *-11* were correlated with attenuation in mice (14). *M. tuberculosis* MmpL4 and MmpL5 were found to transport siderophores that were crucial to cope with iron starvation in a mouse model of infection (60). *M. tuberculosis* MmpL7, -8, -10, and -11 were shown to play a direct role in mycobacterial in vivo survival by shaping the cell wall (61–63).

We show here the reduced production of a previously undescribed glycolipid family, termed glycosyl diacylated nonadecyl diol (GDND), in the absence of MmpL8$_{MAB}$. The cell wall composition and architecture modifications in the $\Delta mmpL8_{MAB}$ mutant, either due to the reduced GDND production and/or altered levels of other lipid species, may explain changes in the interactions between bacteria and MΦ, resulting in decreased intracellular survival and virulence. These cell wall alterations in the $\Delta mmpL8_{MAB}$ mutant might also underlie the lower number of granulomas formed in zebrafish independent of an S$\Delta mmpL8_{MAB}$ or an R$\Delta mmpL8_{MAB}$ infection as already observed with other deletion mutants in *M. abscessus* (33, 51).

A peculiar characteristic of *M. abscessus* is its very large number of MmpL proteins, the highest among 108 mycobacterial strains (31). This observation is particularly striking compared with the SGM MmpL number, with twice the number of MmpLs in the *M. abscessus* clade compared with *M. tuberculosis* complex strains (31). Our phylogenetic studies corroborate these observations by individualizing two *M. abscessus* MmpL-specific clades (blue and red spots in Fig. 2*A*) and by highlighting tandem duplications (blue brackets in Fig. 2*A*).

Several MmpL members from *M. abscessus* clustered with *M. tuberculosis* MmpL proteins as exemplified for MmpL8$_{MAB}$ that clustered with *M. tuberculosis* MmpL8, -10, and -12, although the phylogenetic distance was the highest with MmpL10$_{TB}$. *M. tuberculosis* MmpL10 is involved in the biosynthesis and transport of DATs (64). Its closest homologs in *M. smegmatis* and in *M. abscessus* (*MAB_0937c*) were also reported to transport DATs but did not impact the intracellular persistence of *M. abscessus* (37). We confirm here that *M. tuberculosis mmpL10* fails to complement the intracellular phenotype of $\Delta mmpL8_{MAB}$. Only transcomplementation of $\Delta mmpL8_{MAB}$ with *M. tuberculosis mmpL8* and *-12* restored the WT intracellular phenotype, and this correlated with restoration of GDND production. This complementation is intriguing with regard to the lipid substrate transported. MmpL12 of *M. smegmatis* is involved in the biosynthesis and/or transport of LOS (40), which is no longer functional in *M. tuberculosis* due to genomic reduction (65). Analysis of the syntenic conservation of the *M. abscessus* mmpL8 locus indicated that it is not conserved in *M. smegmatis* but dispersed across its genome (Fig. 2*C*). In *M. smegmatis*, LOSs are presumably transported by MmpL12 (40). However, most of the LOS locus from *M. smegmatis* (*MSMEG_4731–MSMEG_4740*) is not conserved in *M. abscessus* that does not produce LOS. MmpL8 of *M. tuberculosis* is involved in the biosynthesis and/or transport of sulfolipid SL-1 (62), a lipid that is also not present in *M. abscessus*. The restoration of lipid export was not fully in agreement with the intracellular phenotypic behavior for all complemented strains. Considering that the MΦ or amoeba assays are stringent phenotypic assays, this difference reveals subtle substrate differences that might correlate more to the described genetic distances. This point might be solved by purifying each lipid substrate as done for GDND to unravel these differences. In addition, MmpL8$_{MAB}$ and functional equivalent, *M. tuberculosis* MmpL8 and -12, might fulfill another role in addition to transport; they might be involved in the maturation of the exported lipid, a function already reported for *M. tuberculosis* MmpL8 (62).

Of additional interest and to highlight scarcity of homologs of *MAB_0855*, we could not find syntenic conservation of the *mmpL8*$_{MAB}$ region in any other *Mycobacterium*, with the exception of *M. chelonae*, hence providing a unique signature characteristic of the MCC complex. When considering the genes surrounding the locus, synteny was observed only in *M. tuberculosis*, suggesting that the *mmpL8*$_{MAB}$ locus was lost in *M. tuberculosis* as part of the genomic reduction that occurred in the tubercle bacillus.

In the *M. tuberculosis* genome, clusters harboring *pks* genes have been implicated in lipid biosynthesis and assembly (41). Most of these clusters also contain an MmpL-encoding gene that participates in the biosynthesis/export of lipids. In *M. abscessus*, the abundance of MmpL is not associated with a concomitant increase in *pks* genes, suggesting additional roles for MmpL, such as in detoxification or drug efflux mechanisms as reported for *M. tuberculosis* MmpL5 (66) rather than contributing to cell wall elaboration.

From a structural perspective, GDND differs from PDIM by the presence of standard fatty acids (a C19 diol core replacing the phthiocerol and C16/C18 replacing the polymethylated mycocerosic acids) and by the presence of a Glc residue linked to the C19 diol. PDIM represents one of the most important cell wall-associated lipids involved in *M. tuberculosis* virulence (67). Transported by MmpL7$_{MTB}$, it contributes to *M. tuberculosis* escape from the phagosome independent of the pore-forming activity of the ESX-1–secreted substrate EsxA (68). Likewise, PDIM acts in concert with the ESX-1 T7SS (69) to promote phagosomal escape. Notably, our original screen identified the ESX-4 locus as a major contributor to *M. abscessus* virulence in amoebae and MΦ. A deletion mutant of *eccB*$_4$, which encodes a

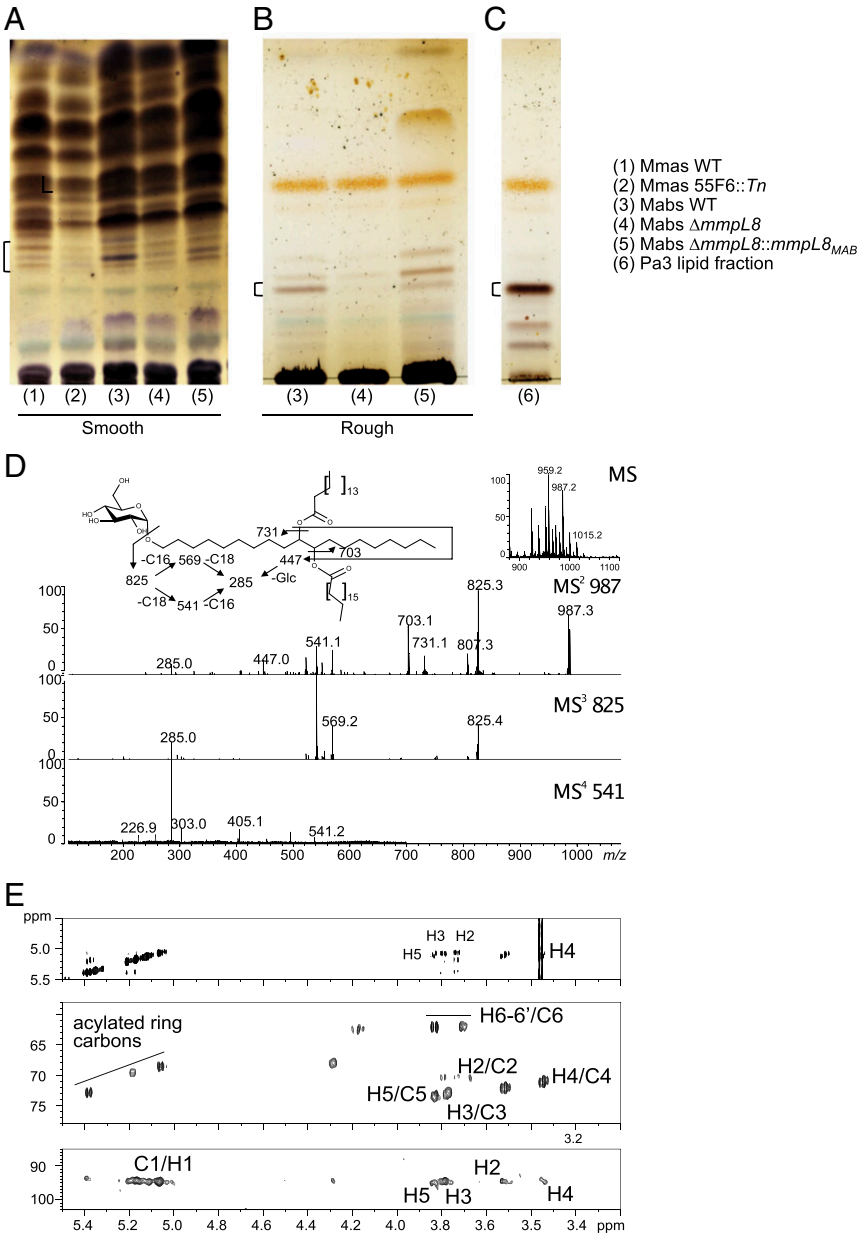


**Fig. 6.** Production of a polar lipid is altered by deletion of *mmpL8*$_{MAB}$. (*A* and *B*) TLC showing a diminished amount of a set of polar lipids in strains lacking *mmpL8*$_{MAB}$. Polar lipids extracted from freeze-dried bacteria (*A*, S strain; *B*, R strain) were separated by TLC using chloroform:methanol:water [90:10:1 (vol/vol/vol)] as the solvent system. TLCs were subsequently stained with orcinol [0.1% (wt/vol) in a 20% (vol/vol) $H_2SO_4$ solution] and charred. The presence of a particular lipid (the lipid with structure that was determined in this study; indicated with brackets) is decreased in the S *Tn MYCMA_0439* mutant and KO *ΔmmpL8*$_{MAB}$ mutant, which is particularly evident in the *M. abscessus* R background lacking GPL. (*C*) TLC of lipids (named Pa3 lipid fraction) from the polar lipid fraction of the R *M. abscessus* strain. The presence of the particular lipid is again indicated with the bracket. (*D*) MALDI-MS and MS$^n$ analyses of purified lipids by successive fragmentations of relevant fragment ions. (Row 1) MALDI-MS spectrum of purified lipid. (Row 2) MS$^2$ fragmentation spectrum of the parent ion at *m/z* 987. (Row 3) MS$^3$ fragmentation spectrum of the fragment ion [M-Hex + H]$^+$ at *m/z* 825. (Row 4) MS$^4$ fragmentation spectrum of the fragment ion [M-Hex-C18 + H]$^+$ at *m/z* 541. On top of the MALDI-MS spectra, the structure of a major component at *m/z* 987 based on MS$^n$, GC-MS, and NMR data is shown. (*E*) Multidimension NMR spectroscopy analysis of the purified lipid. (*Top*) $^1$H/$^1$H TOCSY, (*Middle*) $^1$H/$^{13}$C HSQC, and (*Bottom*) $^1$H/$^{13}$C HSQC-TOCSY NMR spectra showing the spin system of the glycan moiety of the purified lipid.

core structural element of ESX-4, acidified phagosomes and showed reduced signs of phagosome-to-cytosol contacts (39). By analogy with the PDIM/ESX-1 machinery found in *M. tuberculosis*, one may hypothesize that a similar mechanism involving the GDND/ESX-4 system might be used by *M. abscessus* to escape the phagosomal compartment. However, future studies will be required to test this attractive hypothesis.

In conclusion, our study highlights the major role played by MmpL8$_{MAB}$ in controlling *M. abscessus* virulence and production of a family of glycolipids that seems unique to the MCC. As such, this could be considered as the basis of diagnostic markers for pulmonary infections caused by *M. abscessus*.

## Materials and Methods

**Strains, Cells, and Culture Conditions.** Mycobacterial strains were grown aerobically at 37 °C in Middlebrook 7H9 and on 7H11 (Sigma-Aldrich) medium supplemented with 0.2% glycerol and 1% glucose. When necessary, kanamycin, hygromycin (Thermo Fisher Scientific), and zeocin (Thermo Fisher Scientific) were added in the growth medium at 250, 1,000, and 100 μg/mL respectively.

Murine J774.2 (Sigma-Aldrich) MΦ were grown at 37 °C under 5% $CO_2$ in DMEM supplemented with 10% heat-inactivated FCS (FBS; Thermo Fisher Scientific), penicillin (100 IU/mL), and streptomycin (100 IU/mL; Thermo Fisher Scientific).

The human promonocytic cell line, THP-1, was maintained in RPMI 1640 glutamax (Thermo Fisher Scientific) and 10% heat-inactivated FBS at 37 °C under 5% $CO_2$. For differentiation into monocytes, $10^6$ THP-1 cells were seeded into 12-well plates and activated with 20 ng/mL of Phorbol Myristate Acetate (Sigma-Aldrich) for 72 h.

*A. castellanii* (ATCC30010) was grown in PYG Broth (70) for amplification.

***Tn* Mutant Selection and Identification of the *Tn* Insertion.** Selection of *Tn* mutants defective for growth in amoebae and MΦ and identification of the *Tn* insertion site were performed as described previously (39). The *Tn* insertion site was identified by nucleotide BLAST comparison against the *Tn* sequence and the *M. massiliense GO 06* genome hosted by the National Center for Biotechnology Information (NCBI). To confirm the BLAST results, the disrupted region was amplified by PCR using purified genomic DNA obtained from the mutant and a primer that hybridizes within the disrupted gene downstream of the *Tn* insertion site (*SI Appendix*, Table S1).

***MAB_0855* Gene (*mmpL8*$_{MAB}$) and Locus Description.** A motif analysis was performed with InterProScan (71) to confirm that *MAB_0855* belongs to the *mmpL* family, and all proteins encoded by genes from *MAB_0845* to *MAB_0864* were also submitted to InterProScan (71) to check their annotation and to further predict the functions of their corresponding proteins when no functional annotation was provided. *M. abscessus* and *M. tuberculosis mmpL* phylogeny was inferred by Maximum Likelihood using the PHYML software and the approximate likelihood-ratio test (aLRT) statistic. *MAB_0855* and *MAB_0937c* phylogenetic comparison with other mycobacteria was performed by searching putative orthologs with the Opscan program with the "-H" and "-O" options, enabling the identification of a BBH (wwwabi.snv.jussieu.fr/public/opscan/). A list of BHs was obtained by replacing the « -H » option with the « -S » option. BHs displayed a score higher than 40. Conservation of the locus spanning from *MAB_0845* to *MAB_0864* was assessed by a BBH search in the species closest to *M. abscessus*: *M. chelonae* and *M. immunogenum*. Comparisons with saprophytic (*M. smegmatis*), opportunistic (*M. avium*), and strictly pathogenic (*M. tuberculosis*) species were also performed. The loci were drawn with the genoPlotR package (72).

**Construction of the *mmpL8*$_{MAB}$ KO and Relative Complemented Mutants in the *M. abscessus* Subsp. *abscessus* Type Strain.** A KO was performed in the *M. abscessus* subsp. *abscessus* S and R ATCC19977 strains using the recombineering approach (36, 39, 42, 73, 74). Complementation was performed by electrotransforming the mutant strains with the integrative vectors pMVH361::*mmpL8*$_{MAB}$ and pMVH361::*MYCMA_0439*. Complementation studies with the closest homologous *M. tuberculosis* genes to *M. abscessus mmpL8* [*Rv1183* (*MmpL10*$_{MTB}$), *Rv1522c* (*MmpL12*$_{MTB}$), and *Rv3823c* (*MmpL8*$_{MTB}$)] were performed in a similar fashion. Complementation study with the *M. marinum mmpL7*$_{MAR}$ (*MMAR_1764*) gene was also performed in a similar fashion but using the plasmid pMV306.

**Lipid Analyses.** For exploratory systematic lipid analysis, bacteria were cultured in 100 mL LB medium without shaking for 2 wk to obtain mature pellicles. These bacteria were collected by centrifugation, autoclaved, and washed twice with PBS before they were lyophilized. Apolar and polar lipid fractions were extracted from exactly 50 mg of freeze-dried material (R ATCC19977 WT strain) and subsequently analyzed by thin-layer liquid chromatography as previously described (75). For lipid purifications, exponentially growing bacteria (S and R ATCC19977 WT, Δ*mmpL8*, and complemented strains) were plated on 7H10$^{OADC}$ agar plates (100 μL per plate) and incubated for 1 wk at 37 °C until a dense lawn of bacterial growth was obtained. Subsequently, bacteria were collected using an inoculation loop, suspended in PBS, autoclaved for 10 min at 121 °C, washed thrice with PBS, flash frozen in liquid nitrogen, and freeze dried. Apolar and polar lipid fractions were then obtained, and polar lipids were fractionated by two rounds of liquid flash chromatography on a silica gel column (80 g, 50 mm) using a chloroform:MeOH gradient (100:0–40:60). The lipid of interest was finally purified by preparative TLC in chloroform:methanol [9:1 (vol/vol)]. Monosaccharide composition was established by GC-flame ionization detector (FID) and GC-MS analyses of trimethylsilylated methylglycosides according to Kamerling et al. (76) using mesoinositol and scylloinositol as internal standards. Fatty acids were released by methyl esterification with 0.5 M HCl in anhydrous methanol at 80 °C for 20 h, extracted with heptane, and identified by GC-MS as fatty acid methyl esters. Intact glycolipids were sequenced by MS$^n$ using an Axima Resonance MALDI quadrupole ion trap TOF instrument (Shimadzu). The sample was dissolved in chloroform: methanol [9:1 (vol/vol)] and mixed with 1 vol of a solution of 10 mg 2,5-dihydroxybenzoic acid in 1 mL chloroform:methanol [2:1 (vol/vol)] before spotting on an MALDI plate. The instrument was operated in positive ion and reflectron mode. Fragment ions were analyzed by collision-induced dissociation of the precursor ions, and argon was used as a collision gas. Before NMR spectroscopic analyses, the sample was repeatedly exchanged in $CDCl_3$:$CD_3OD$ [2:1 (vol/vol); 99.97% purity; Eurisotop-Saclay] with intermediate drying and then dissolved in $CDCl_3$:$CD_3OD$ [2:1 (vol/vol)]. Solution-state NMR experiments were recorded at 300 K on a Bruker Avance 900 spectrometer equipped with a 3-mm triple-resonance cryoprobe using Bruker standard pulse programs.

**Infection, Adhesion, and Phagosomal Escape Assays.** MΦ infection experiments with the WT, Δ*mmpL8*, and complemented strains were performed as described (4, 42).

Adhesion experiments to murine MΦ were performed by flow cytometry based on the method described by Hytönen et al. (77). Before infection, log-phase bacteria were stained with CFDA-SE 50 μM (Molecular Probes; Thermo Fisher Scientific) for 20 min at 37 °C with end-over-end rotation, washed twice with cold PBS, and kept on ice protected from light. In the meantime, MΦ were washed twice with DMEM, scraped, and resuspended in DMEM. The cells were incubated at 4 °C for 30 min with gentle agitation before the infection; 50,000 cells were infected with the bacterial strains at a high multiplicity of infection (MOI) of 100 to favor bacteria-to-cell contacts and then incubated at 4 °C for 45 min with gentle agitation. The cell–bacteria incubations were carried out in three parallel tubes, and the experiments were repeated twice with new batches of MΦ and labeled bacteria. The fluorescence intensity of the cells with adherent bacteria was measured with BD Fortessa equipment (Becton Dickinson Biosciences). The data obtained from the flow cytometer were analyzed using BD FACSDIVA software and the FlowJo software.

Phagosome acidification and phagosomal escape FRET assays were conducted in THP-1 cells as previously described (78).

**Cytokine Assays.** IL-1β secretion was measured as previously described (79).

The FAM-FLICA caspase-1 Assay Kit (ImmunoChemistry Technologies) was used to evaluate the presence of catalytically active forms of caspase-1 p10 and p12. THP-1 cells were infected at an MOI of 10 for 3 h. As a positive control of apoptosis induction, cells were incubated with 500 nM LPS for 8 h at 37 °C. The adherent cells were gently dissociated with TrypLE Express reagent (Gibco; Thermo Fisher Scientific) as recommended. Cells were washed twice and resuspended in RPMI medium with 10% FBS before staining with 30×XFam-Vad-Fmk for 30 min at 37 °C. To gate specifically on differentiated intact cells, the cells were also stained with the CD11b antibody (78) before treatment with 5% paraformaldehyde (PFA). Fixed cells were then analyzed by flow cytometry. The results are expressed as the percentage of cells harboring the caspase-1 p10 and p12 active forms.

**Zebrafish Infections.** All zebrafish protocols adhered to the guidelines specified by the Direction Sanitaire et Vétérinaire de l'Hérault et Comité d'Ethique pour l'Expérimentation Animale de la région Languedoc Roussillon under the reference CEEA-LR-1145. All efforts were made to minimize pain and discomfort according to European animal welfare regulations and standard protocols. Infection experiments were done using tdTomato-expressing *M. abscessus* strains and performed as described previously (28). Mortality was determined by recording the number of dead embryos daily. To evaluate granuloma formation, embryos at 5 dpi were embedded in 1% low melting point agarose and transferred to a Zeiss microscope with a Zeiss Plan NeoFluar Z 1×/0.25 objective for monitoring.

**Culture for Cording.** In total, 4 million cfu of mycobacteria were cultured in 1 mL of 7H9 supplemented with 1% glucose in a 24-well plate at 37 °C without agitation until visualization of a bacterial film on the surface of the medium. The plates were sealed with parafilm to avoid evaporation. The formation of cords was checked by observation with an optical microscope (*SI Appendix*, Fig. S5).

**ACKNOWLEDGMENTS.** We thank B. Maury for cytometry settings. V.D. was supported by French Cystic Fibrosis Patients Association Vaincre la Mucoviscidose Grant RF20150501377. This work was supported by Fondation pour la Recherche Médicale Grant DEQ20150331719 (to L.K.) and Agence National de la Recherche Grant MyCat ANR-15-CE18-0007-01 (to Y.G. and L.K.).

1. Glickman MS, Cox JS, Jacobs WR, Jr (2000) A novel mycolic acid cyclopropane synthetase is required for cording, persistence, and virulence of Mycobacterium tuberculosis. *Mol Cell* 5:717–727.
2. Makinoshima H, Glickman MS (2005) Regulation of Mycobacterium tuberculosis cell envelope composition and virulence by intramembrane proteolysis. *Nature* 436:406–409.
3. Brambilla C, et al. (2016) Mycobacteria clumping increase their capacity to damage macrophages. *Front Microbiol* 7:1562.
4. Roux A-L, et al. (2016) The distinct fate of smooth and rough Mycobacterium abscessus variants inside macrophages. *Open Biol* 6:160185.
5. Singh P, Rameshwaram NR, Ghosh S, Mukhopadhyay S (2018) Cell envelope lipids in the pathophysiology of *Mycobacterium tuberculosis*. *Future Microbiol* 13:689–710.
6. Jackson M (2014) The mycobacterial cell envelope-lipids. *Cold Spring Harb Perspect Med* 4:a021105.
7. Gutiérrez AV, Viljoen A, Ghigo E, Herrmann J-L, Kremer L (2018) Glycopeptidolipids, a double-edged sword of the *Mycobacterium abscessus* complex. *Front Microbiol* 9:1145.
8. Cole ST, et al. (1998) Deciphering the biology of Mycobacterium tuberculosis from the complete genome sequence. *Nature* 393:537–544.
9. Kaur D, Guerin ME, Skovierová H, Brennan PJ, Jackson M (2009) Chapter 2: Biogenesis of the cell wall and other glycoconjugates of Mycobacterium tuberculosis. *Adv Appl Microbiol* 69:23–78.
10. Brennan PJ (2003) Structure, function, and biogenesis of the cell wall of Mycobacterium tuberculosis. *Tuberculosis (Edinb)* 83:91–97.

11. Cox JS, Chen B, McNeil M, Jacobs WR, Jr (1999) Complex lipid determines tissue-specific replication of Mycobacterium tuberculosis in mice. *Nature* 402:79–83.
12. Yu J, et al. (2012) Both phthiocerol dimycocerosates and phenolic glycolipids are required for virulence of Mycobacterium marinum. *Infect Immun* 80:1381–1389.
13. Cambier CJ, et al. (2014) Mycobacteria manipulate macrophage recruitment through coordinated use of membrane lipids. *Nature* 505:218–222.
14. Domenech P, Reed MB, Barry CE, 3rd (2005) Contribution of the Mycobacterium tuberculosis MmpL protein family to virulence and drug resistance. *Infect Immun* 73:3492–3501.
15. Alibaud L, et al. (2011) A Mycobacterium marinum TesA mutant defective for major cell wall-associated lipids is highly attenuated in Dictyostelium discoideum and zebrafish embryos. *Mol Microbiol* 80:919–934.
16. Belisle JT, Pascopella L, Inamine JM, Brennan PJ, Jacobs WR, Jr (1991) Isolation and expression of a gene cluster responsible for biosynthesis of the glycopeptidolipid antigens of Mycobacterium avium. *J Bacteriol* 173:6991–6997.
17. Pawlik A, et al. (2013) Identification and characterization of the genetic changes responsible for the characteristic smooth-to-rough morphotype alterations of clinically persistent Mycobacterium abscessus. *Mol Microbiol* 90:612–629.
18. Sondén B, et al. (2005) Gap, a mycobacterial specific integral membrane protein, is required for glycolipid transport to the cell surface. *Mol Microbiol* 58:426–440.
19. Billman-Jacobe H (2004) Glycopeptidolipid synthesis in mycobacteria. *Curr Sci* 86: 111–114.
20. Byrd TF, Lyons CR (1999) Preliminary characterization of a Mycobacterium abscessus mutant in human and murine models of infection. *Infect Immun* 67:4700–4707.
21. Catherinot E, et al. (2009) Acute respiratory failure involving an R variant of Mycobacterium abscessus. *J Clin Microbiol* 47:271–274.
22. Bernut A, et al. (2016) Insights into the smooth-to-rough transitioning in Mycobacterium bolletii unravels a functional Tyr residue conserved in all mycobacterial MmpL family members. *Mol Microbiol* 99:866–883.
23. Bernut A, Herrmann J-L, Ordway D, Kremer L (2017) The diverse cellular and animal models to decipher the physiopathological traits of *Mycobacterium abscessus* infection. *Front Cell Infect Microbiol* 7:100.
24. Kreutzfeldt KM, et al. (2013) Molecular longitudinal tracking of Mycobacterium abscessus spp. during chronic infection of the human lung. *PLoS One* 8:e63237.
25. Jönsson BE, et al. (2007) Molecular epidemiology of Mycobacterium abscessus, with focus on cystic fibrosis. *J Clin Microbiol* 45:1497–1504.
26. Qvist T, et al. (2016) Comparing the harmful effects of nontuberculous mycobacteria and Gram negative bacteria on lung function in patients with cystic fibrosis. *J Cyst Fibros* 15:380–385.
27. Catherinot E, et al. (2007) Hypervirulence of a rough variant of the Mycobacterium abscessus type strain. *Infect Immun* 75:1055–1058.
28. Bernut A, et al. (2014) Mycobacterium abscessus cording prevents phagocytosis and promotes abscess formation. *Proc Natl Acad Sci USA* 111:E943–E952.
29. Whang J, et al. (2017) Mycobacterium abscessus glycopeptidolipids inhibit macrophage apoptosis and bacterial spreading by targeting mitochondrial cyclophilin D. *Cell Death Dis* 8:e3012.
30. Brosch R, et al. (2000) Comparative genomics of the mycobacteria. *Int J Med Microbiol* 290:143–152.
31. Viljoen A, et al. (2017) The diverse family of MmpL transporters in mycobacteria: From regulation to antimicrobial developments. *Mol Microbiol* 104:889–904.
32. Chalut C (2016) MmpL transporter-mediated export of cell-wall associated lipids and siderophores in mycobacteria. *Tuberculosis (Edinb)* 100:32–45.
33. Dupont C, et al. (2016) A new piperidinol derivative targeting mycolic acid transport in Mycobacterium abscessus. *Mol Microbiol* 101:515–529.
34. Kozikowski AP, et al. (2017) Targeting mycolic acid transport by Indole-2-carboxamides for the treatment of Mycobacterium abscessus infections. *J Med Chem* 60:5876–5888.
35. Viljoen A, et al. (2017) Controlling extra- and intramacrophagic *Mycobacterium abscessus* by targeting mycolic acid transport. *Front Cell Infect Microbiol* 7:388.
36. Medjahed H, Reyrat J-M (2009) Construction of Mycobacterium abscessus defined glycopeptidolipid mutants: Comparison of genetic tools. *Appl Environ Microbiol* 75:1331–1338.
37. Burbaud S, et al. (2016) Trehalose polyphleates are produced by a glycolipid biosynthetic pathway conserved across phylogenetically distant mycobacteria. *Cell Chem Biol* 23:278–289.
38. Llorens-Fons M, et al. (2017) Trehalose polyphleates, external cell wall lipids in Mycobacterium abscessus, are associated with the formation of clumps with cording morphology, which have been associated with virulence. *Front Microbiol* 8:1402.
39. Laencina L, et al. (2018) Identification of genes required for *Mycobacterium abscessus* growth in vivo with a prominent role of the ESX-4 locus. *Proc Natl Acad Sci USA* 115: E1002–E1011.
40. Etienne G, et al. (2009) Identification of the polyketide synthase involved in the biosynthesis of the surface-exposed lipooligosaccharides in mycobacteria. *J Bacteriol* 191:2613–2621.
41. Kolattukudy PE, Fernandes ND, Azad AK, Fitzmaurice AM, Sirakova TD (1997) Biochemistry and molecular genetics of cell-wall lipid biosynthesis in mycobacteria. *Mol Microbiol* 24:263–270.
42. Bakala N'Goma JC, et al. (2015) Mycobacterium abscessus phospholipase C expression is induced during coculture within amoebae and enhances M. abscessus virulence in mice. *Infect Immun* 83:780–791.
43. Medjahed H, Singh AK (2010) Genetic manipulation of Mycobacterium abscessus. *Curr Protoc Microbiol* Chapter 10:Unit 10D.2.
44. Pethe K, et al. (2004) Isolation of Mycobacterium tuberculosis mutants defective in the arrest of phagosome maturation. *Proc Natl Acad Sci USA* 101:13642–13647.
45. Queval CJ, Brosch R, Simeone R (2017) The macrophage: A disputed fortress in the battle against *Mycobacterium tuberculosis*. *Front Microbiol* 8:2284.
46. Collins AC, et al. (2015) Cyclic GMP-AMP synthase is an innate immune DNA sensor for Mycobacterium tuberculosis. *Cell Host Microbe* 17:820–828.
47. Kupz A, et al. (2016) ESAT-6-dependent cytosolic pattern recognition drives noncognate tuberculosis control in vivo. *J Clin Invest* 126:2109–2122.
48. Wassermann R, et al. (2015) Mycobacterium tuberculosis differentially activates cGAS- and inflammasome-dependent intracellular immune responses through ESX-1. *Cell Host Microbe* 17:799–810.
49. Watson RO, et al. (2015) The cytosolic sensor cGAS detects Mycobacterium tuberculosis DNA to induce type I interferons and activate autophagy. *Cell Host Microbe* 17: 811–819.
50. Bernut A, et al. (2015) Deciphering and imaging pathogenesis and cording of Mycobacterium abscessus in zebrafish embryos. *J Vis Exp* 103:e53130.
51. Halloum I, et al. (2016) Deletion of a dehydratase important for intracellular growth and cording renders rough Mycobacterium abscessus avirulent. *Proc Natl Acad Sci USA* 113:E4228–E4237.
52. Indrigo J, Hunter RL, Jr, Actor JK (2003) Cord factor trehalose 6,6′-dimycolate (TDM) mediates trafficking events during mycobacterial infection of murine macrophages. *Microbiology* 149:2049–2059.
53. Andréjak C, et al. (2013) Chronic respiratory disease, inhaled corticosteroids and risk of non-tuberculous mycobacteriosis. *Thorax* 68:256–262.
54. Chu H, et al. (2014) Prevalence of nontuberculous mycobacteria in patients with bronchiectasis: A meta-analysis. *Arch Med Sci* 10:661–668.
55. Olivier KN, et al.; Nontuberculous Mycobacteria in Cystic Fibrosis Study Group (2003) Nontuberculous mycobacteria. I. Multicenter prevalence study in cystic fibrosis. *Am J Respir Crit Care Med* 167:828–834.
56. Floto RA, et al. (2016) US cystic fibrosis foundation and European cystic fibrosis society consensus recommendations for the management of non-tuberculous mycobacteria in individuals with cystic fibrosis: Executive summary. *Thorax* 71:88–90.
57. Chan ED, Iseman MD (2013) Underlying host risk factors for nontuberculous mycobacterial lung disease. *Semin Respir Crit Care Med* 34:110–123.
58. Park IK, Olivier KN (2015) Nontuberculous mycobacteria in cystic fibrosis and noncystic fibrosis bronchiectasis. *Semin Respir Crit Care Med* 36:217–224.
59. Lamichhane G, Tyagi S, Bishai WR (2005) Designer arrays for defined mutant analysis to detect genes essential for survival of Mycobacterium tuberculosis in mouse lungs. *Infect Immun* 73:2533–2540.
60. Wells RM, et al. (2013) Discovery of a siderophore export system essential for virulence of Mycobacterium tuberculosis. *PLoS Pathog* 9:e1003120.
61. Jain M, Cox JS (2005) Interaction between polyketide synthase and transporter suggests coupled synthesis and export of virulence lipid in M. tuberculosis. *PLoS Pathog* 1:e2.
62. Converse SE, et al. (2003) MmpL8 is required for sulfolipid-1 biosynthesis and Mycobacterium tuberculosis virulence. *Proc Natl Acad Sci USA* 100:6121–6126.
63. Pacheco SA, Hsu F-F, Powers KM, Purdy GE (2013) MmpL11 protein transports mycolic acid-containing lipids to the mycobacterial cell wall and contributes to biofilm formation in Mycobacterium smegmatis. *J Biol Chem* 288:24213–24222.
64. Belardinelli JM, et al. (2014) Biosynthesis and translocation of unsulfated acyltrehaloses in Mycobacterium tuberculosis. *J Biol Chem* 289:27952–27965.
65. Boritsch EC, et al. (2016) pks5-recombination-mediated surface remodelling in Mycobacterium tuberculosis emergence. *Nat Microbiol* 1:15019.
66. Briffotaux J, Huang W, Wang X, Gicquel B (2017) MmpS5/MmpL5 as an efflux pump in Mycobacterium species. *Tuberculosis (Edinb)* 107:13–19.
67. Astarie-Dequeker C, et al. (2009) Phthiocerol dimycocerosates of M. tuberculosis participate in macrophage invasion by inducing changes in the organization of plasma membrane lipids. *PLoS Pathog* 5:e1000289.
68. Quigley J, et al. (2017) The cell wall lipid PDIM contributes to phagosomal escape and host cell exit of *Mycobacterium tuberculosis*. *MBio* 8:e00148-17.
69. Augenstreich J, et al. (2017) ESX-1 and phthiocerol dimycocerosates of *Mycobacterium tuberculosis* act in concert to cause phagosomal rupture and host cell apoptosis. *Cell Microbiol* 19:e12726.
70. Rowbotham TJ (1983) Isolation of Legionella pneumophila from clinical specimens via amoebae, and the interaction of those and other isolates with amoebae. *J Clin Pathol* 36:978–986.
71. Quevillon E, et al. (2005) InterProScan: Protein domains identifier. *Nucleic Acids Res* 33:W116–W120.
72. Guy L, Kultima JR, Andersson SGE (2010) genoPlotR: Comparative gene and genome visualization in R. *Bioinformatics* 26:2334–2335.
73. Le Moigne V, et al. (2016) MgtC as a host-induced factor and vaccine candidate against Mycobacterium abscessus infection. *Infect Immun* 84:2895–2903.
74. van Kessel JC, Hatfull GF (2007) Recombineering in Mycobacterium tuberculosis. *Nat Methods* 4:147–152.
75. Besra GS (1998) Preparation of cell-wall fractions from Mycobacteria. *Mycobacteria Protocols*, eds Parish T, Stoker NG (Humana, Totowa, NJ), Vol 101, pp 91–108.
76. Kamerling JP, Gerwig GJ, Vliegenthart JF, Clamp JR (1975) Characterization by gas-liquid chromatography-mass spectrometry and proton-magnetic-resonance spectroscopy of pertrimethylsilyl methyl glycosides obtained in the methanolysis of glycoproteins and glycopeptides. *Biochem J* 151:491–495.
77. Hytönen J, Haataja S, Finne J (2006) Use of flow cytometry for the adhesion analysis of Streptococcus pyogenes mutant strains to epithelial cells: Investigation of the possible role of surface pullulanase and cysteine protease, and the transcriptional regulator Rgg. *BMC Microbiol* 6:18.
78. Simeone R, et al. (2015) Cytosolic access of Mycobacterium tuberculosis: Critical impact of phagosomal acidification control and demonstration of occurrence in vivo. *PLoS Pathog* 11:e1004650.
79. Gröschel MI, et al. (2017) Recombinant BCG expressing ESX-1 of Mycobacterium marinum combines low virulence with cytosolic immune signaling and improved TB protection. *Cell Rep* 18:2752–2765.